International Journal of Mass Spectrometry 406 (2016) 55–61

Contents lists available at ScienceDirect

International Journal of Mass Spectrometry

journal homepage: www.elsevier.com/locate/ijms

An aplanatic-lens velocity map imaging spectrometer with improved kinetic energy resolution for photoions

Peng Zhang[a], Min Li[a,*], Siqiang Luo[a], Yueming Zhou[a], Qingbin Zhang[a], Pengfei Lan[a,*], Peixiang Lu[a,b]

[a] School of Physics and Wuhan National Laboratory for Optoelectronics, Huazhong University of Science and Technology, Wuhan 430074, China
[b] Laboratory of Optical Information Technology, Wuhan Institute of Technology, Wuhan 430074, China

ARTICLE INFO

Article history:
Received 9 April 2016
Received in revised form 8 June 2016
Accepted 13 June 2016
Available online 15 June 2016

ABSTRACT

We propose a new method to improve the energy resolution of photoions with an aplanatic velocity map imaging spectrometer. Building on the traditional VMI spectrometer with three aperture electrodes, we apply a stepped voltage on the extractor electrode of the spectrometer to reduce the spherical aberration effect of the electrostatic lens. This stepped voltage acts as a diverging electrostatic lens in ion optics. A combination of the converging electrostatic lens and the subsequent diverging electrostatic lens constitutes an aplanatic electrostatic lens. With precisely controlling the moment of the voltage, we suppress the spherical aberration effect induced by the converging electrostatic lens in the traditional VMI spectrometer. Both simulated and experimental results demonstrate that the energy resolution is significantly improved using this aplanatic-lens VMI spectrometer.

1. Introduction

Atoms and molecules exposed to strong laser fields will lead to many interesting strong-field phenomena such as above-threshold ionization [1], tunnel ionization [2,3], sequential or nonsequential double ionization [4–6], high-order harmonic generation [7,8] and molecular dissociation [9,10]. All of those phenomena can be used to retrieve the atomic and molecular information and dynamics [11,12]. Velocity map imaging (VMI) technique [13], developed by Eppink and Parker in 1997, is powerful in investigating the underlying dynamics of the dissociation, ionization and molecular collisions [14–16]. Experimentally, the VMI technique has been widely used in photoelectron holography [17–19], electron wavepacket interference [20,21], molecular orbital imaging [22,23], etc. In a typical velocity map imaging setup, the products resulting from the dissociation or the ionization processes are focused onto a two dimensional detector with an electrostatic lens configuration. In general, the detector consists of dual micro-channel plates, a phosphor screen, and a CCD camera. A 2D image is recorded on the detector, where the radial of the image is proportional to particle velocity and the intensity distribution around the azimuth is indicative of the angular distribution. In a linearly polarized laser field, the 3D initial velocity distribution of the generated particles is cylindrically symmetric. With some retrieval algorithms [24–26], the 3D initial velocity distribution can be reconstructed from the 2D raw image.

The energy resolution of the VMI setup stands as a crucial parameter for accurately imaging the atomic and molecular dynamics. A high kinetic energy (KE) resolution will provide an unambiguous image for strong-field atomic and molecular process, which is especially vital for some fine structures in the energy spectrum. For instance, the multiphoton ionization of some atoms and molecules shows some resonant peaks which are very close to each other in the photoelectron KE spectra [27–29]. In addition, Stark splitting also induces some fine structures in the photoelectron KE spectra [30,31].

In VMI spectrometers, with the electrostatic lens, the ions or electrons which origin from different positions with the same initial velocity vector are mapped to the same point in the focal plane. Thus the resolution of the ion imaging technique was dramatically enhanced. Since the use of the VMI, many works has been reported with high resolution [34–36]. A KE resolution as good as 0.38% has been reported by Maurice H. M. Janssen et al. in 2005 [35]. However, the aberration effect of the electrode lens in VMI has a crucial effect on the resolution of the image [37]. This effect is also found in imaging techniques using ion/electron optics, such as the spherical aberration effect in transmission electron microscopy (TEM) [32] and ultracold ion source [33]. The spherical aberration effect in VMI

* Corresponding authors.
E-mail addresses: mli@hust.edu.cn (M. Li), pengfeilan@hust.edu.cn (P. Lan).

http://dx.doi.org/10.1016/j.ijms.2016.06.006
1387-3806/

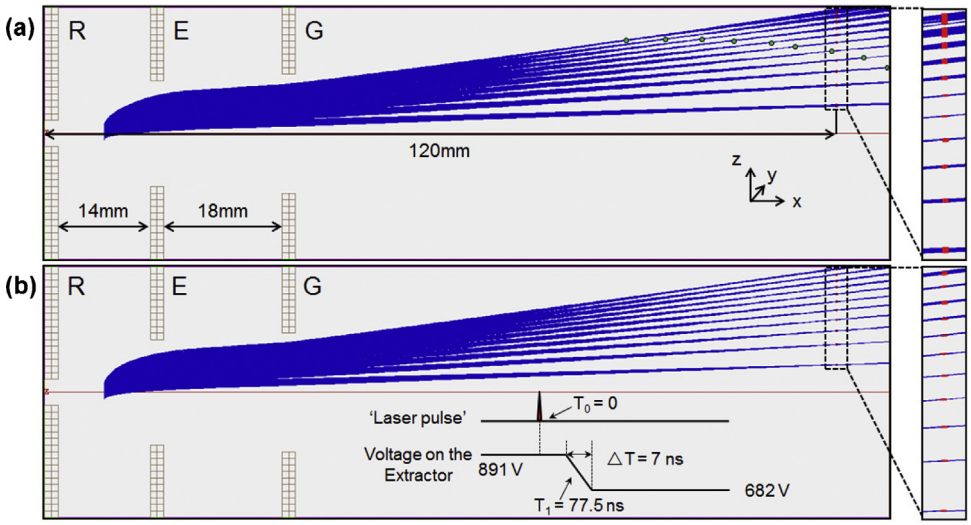

Fig. 1. Cross-sections of the traditional VMI spectrometer and the AL-VMI spectrometer. Blue lines are the trajectory of the ions. The red spots are the intersection points of the particles' trajectories with the detector. The green points are focuses of the ions, noting that the focuses (green points) in the bottom drawing are not shown for overlapping with the detector. In the two imaging spectrometers, the distances between the detector and the repeller electrode are identical. The two right panels show the enlarged view of the spots on the detectors. The electrodes' setups, which can be found in the figure, of the two imaging spectrometers are same as each other. R = repeller, E = extractor and G = grounded electrode. (a) Cross-section of the traditional VMI spectrometer. (b) Cross-section of the AL-VMI spectrometer. The inset is the voltage that we applied on the extractor and its timing match with the laser pulse in the AL-VMI spectrometer. (For interpretation of the references to colour in this figure legend, the reader is referred to the web version of this article.).

manifests itself as the particles with different KE reaching a velocity focus at different positions along the time-of-flight direction. This effect leads to a "v" shaped dispersion [38] of the KE resolution, i.e., the resolution for ions with low KE and high KE is worse than that with the medium KE.

In recent years, several methods are proposed to improve the resolution of the spectrometer [39–41]. S. Skruszewicz et al. have designed a high energy VMI, in which two electrodes are added into the traditional VMI spectrometer [39]. The two additional electrodes act as another two concave electrostatic lenses. With the two additional electrostatic lenses, the ions/electrons can be squeezed further to the spectrometer axis thus increasing the KE measurement range of the spectrometer. This design could also improve the resolution of the photoelectrons. Another design called thick-lens VMI was proposed by N.G. Kling et al., who extends the applied electric field using 11 electrodes to form a thick electrostatic lens [41]. This permits measurements of the charged particles with higher KE while achieving a good resolution over a wide range of KE. However, this spectrometer consists by up to 11 electrodes, which is complicated for construction and adjustment. In this article, we introduce a much simpler method to improve the KE resolution of the ion images. On the basis of the configuration of the traditional VMI, we apply a stepped voltage on the extractor electrode to avoid the spherical aberration effect of the electrostatic lens. This stepped voltage acts as a diverging electrostatic lens. The intrinsic converging electrostatic lens and the subsequent diverging electrostatic lens constitute an aplanatic electrostatic lens. Through careful modelling and measurements of the ion images, we demonstrate the energy resolution can be significantly improved using this aplanatic lens VMI (AL-VMI). This paper is organized as follows. In Section 2, we investigate the performance of the AL-VMI spectrometer by simulation. The experimental implementation of the AL-VMI spectrometer is shown in Section 3. The discussion and conclusion of this paper are given in Section 4.

2. Simulations

We first show a typical VMI setup in Fig. 1(a). The spectrometer of the VMI consists of three plates with aperture electrodes. The distance between the repeller (R) electrode and the extractor (E) electrode is 14 mm, between the extractor electrode and the ground (G) electrode is 18 mm, and between the repeller electrode and the detector plane is 120 mm. The interaction region of the "laser" and the "molecular beam" is located in the middle of the electrodes R and E. The "laser" is linearly polarized along the *z*-axis and propagates along the *y*-axis. The ions' trajectories in the VMI spectrometer can be simulated using SIMION v. 8.0 [42]. The blue curves in Fig. 1(a) are the ions' trajectories with different KE. Here we have assumed that the size of the interaction region along the *y*-axis is 1.0 mm, and the size along the *x*-axis, which corresponds to the minimum beam waist of the "laser", is 10.0 μm. The initial KE ranges from 0.5 eV to 10.5 eV with an interval of 1 eV. This KE range of the ions is common in a typical VMI experiment. The initial velocity of the ions is along the *z* axis. A voltage of +740.5 V is applied on the repeller electrode and a voltage of +565 V on the extractor electrode. The focuses of the ion beams for different energies are labeled with green spots in Fig. 1(a). From Fig. 1(a), it can be clearly seen that the ions with high KE are focused earlier than that with low KE. In fact, this phenomenon is induced by the spherical aberration effect of the electrostatic lens. In the VMI spectrometer, ions with high KE fly through the edge of the electrostatic lens, while ions with low KE fly through the center of the electrostatic lens. Due to the spherical aberration effect, the ions with high KE flying away from the central line will be focused earlier than that with low KE flying near the central line. Generally, the detector plane is placed near the focus point of ions with the medium KE. Thus, on the detector plane, one can see that the width of the mapped ion distribution (labeled with red spots in Fig. 1) is minimum for ions with medium KE and it becomes very large for ions with low KE or high KE, i.e., the resolution for ions with low KE and high KE is worse than that with the medium KE. In short, the KE resolution of the VMI spectrometer decreases because of the spherical aberration effect.

To reduce the influence of the spherical aberration, we apply a stepped voltage on the extractor electrode instead of constant voltage for the traditional VMI. A similar method has been successfully used in transmission electron microscopy (TEM) [43] and ultracold ion source [33] to reduce the spherical aberration effect. Using

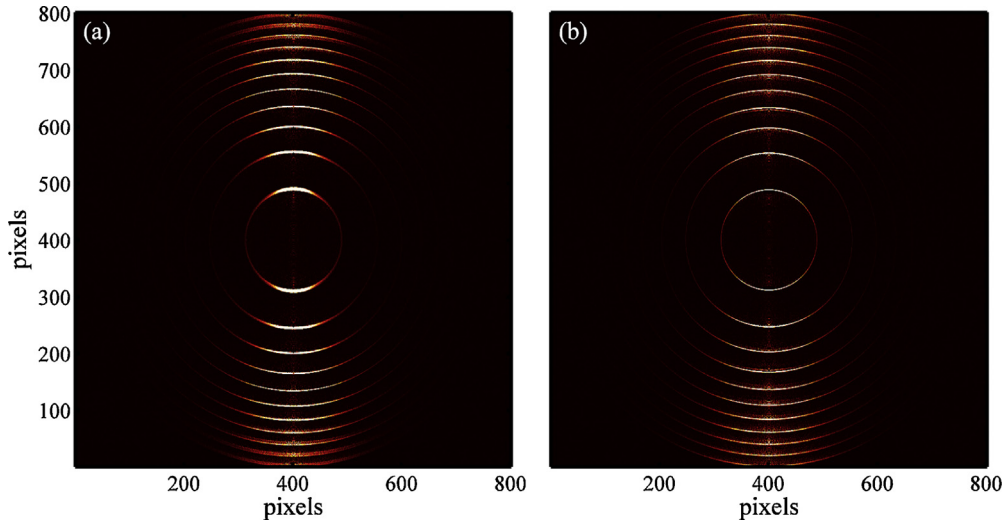

Fig. 2. Simulation results: the 2D cuts of the 3D images reconstructed by BASEX method of (a) the traditional VMI and (b) the AL-VMI.

this stepped voltage, the spherical aberration can be well compensated, and the ions which fly near the central line or away from the central line of the electrode lens can be focused at the same plane perpendicular to the time-of-flight axis. Thus the KE resolution of the spectrometer can be improved. The VMI technique using this aplanatic method is dubbed aplanatic lens VMI (AL-VMI) in this paper. We simulate the ions' trajectories with the AL-VMI in Fig. 1(b) with the same conditions as the traditional VMI shown in Fig. 1(a). *Vr* is set to be +1000 V and *Ve* is primarily set to +890.5 V then it is switched to +682 V at 77.5 ns after the "ionization". The duration of the switch process is assumed to be 7 ns. The voltage of the repeller and extractor electrodes are set to keep the maximum impinge position on the detector is nearly the same for Fig. 1(a) and (b). From Fig. 1(b), due to the use of the stepped voltage, the ion beams (blue) of the whole KE range focus on nearly the same plane perpendicular to the *x* axis. Furthermore, the sizes of the spots on the detector plane are very small and keep nearly unchanged with the increase of the KE, as compared with the traditional VMI shown in Fig. 1(a). Because of the fast step of the lens potential at a specific time, the ions are accelerated and therefore slightly diverged. Ions with off-axis trajectories are deflected more by the change in potential and subsequently reach a focus further away, thus it acts as a diverging electrostatic lens. The intrinsic converging electrostatic lens and the subsequent diverging electrostatic lens constitute an aplanatic electrostatic lens. Thus, the spherical aberration is well compensated in the AL-VMI spectrometer.

We further investigate the performance of the AL-VMI by adopting a 3D cylindrically distribution as the initial velocity distribution in the simulation. Generally, the driving laser field is linearly polarized. The interaction of the linearly polarized laser field and a molecular beam produces a 3D initial velocity distribution, and the distribution is cylindrically symmetric around the polarization axis of the laser field. Using SIMION, we simulate the flight trajectories with an ensemble of 3.0×10^6 ions. The mass of the ions in the simulation is 1.008 amu., which is the relative atom mass of H^+. The input KE of the ions ranges from 0.5 eV to 9.5 eV with an interval of 1 eV and is set to be the same for the two VMI spectrometers. After "ionization", the ions were projected to the detector by the ion optics, and their positions recorded to generate the simulated velocity-map image. With the basis set expansion (BASEX) Abel inversion method [25], we reconstruct the initial 3D velocity distribution from the 2D raw image. The 2D cuts of the 3D distributions are shown in Fig. 2(a) and (b) with the traditional VMI and AL-VMI, respectively. From Fig. 2, one can clearly see many sharp rings, corresponding to the ions with different KE. Because the AL-VMI mainly improves the KE resolution for the low KE and the high KE parts, we show in Fig. 3 the enlarged views of the low and high KE parts of Fig. 2. One can find that the rings reconstructed from AL-VMI [shown in Fig. 3(b) and (d)] are sharper than those from the traditional VMI [shown in Fig. 3(a) and (c)]. In other words, the KE rings reconstructed from AL-VMI are easier to be distinguished. In Fig. 4(a)–(c), we compare the KE distribution retrieved by the

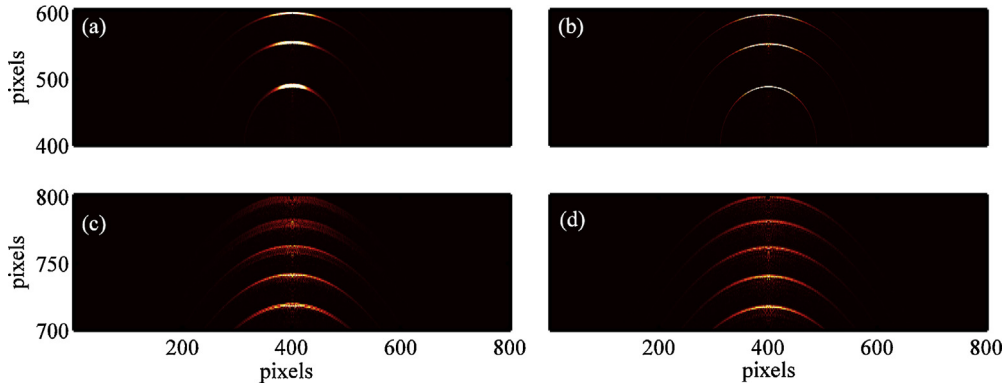

Fig. 3. The enlarged views of the low and high KE parts of Fig. 2. (a) the low KE part of the traditional VMI. (b) the low KE part of AL-VMI. (c) the high KE part of the traditional VMI. (d) the high KE part of AL-VMI.

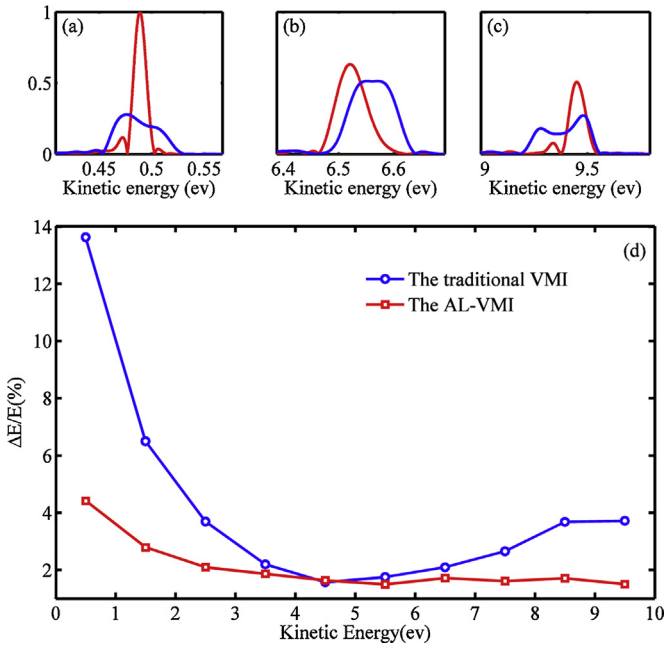

Fig. 4. Simulation results: (a)–(c) The KE distribution of the traditional VMI (blue) and AL-VMI (red) at 0.5 eV, 6.5 eV and 9.5 eV respectively. (d) the KE resolution of the traditional VMI (blue) and the AL-VMI (red) at different KE. (For interpretation of the references to colour in this figure legend, the reader is referred to the web version of this article.).

traditional VMI and AL-VMI at 0.5 eV, 6.5 eV, and 9.5 eV, which correspond to the low KE, the medium KE and the high KE parts of Fig. 2, respectively. At 6.5 eV, the peaks of both spectrometers are sharp, and the peak width of the AL-VMI is a little narrower than that of the traditional VMI. At 0.5 eV and 9.5 eV, it can be found that the peaks of the traditional VMI are very broad, and the peaks of the AL-VMI are narrower and higher than those of the traditional VMI. To quantitatively figure out the KE resolutions of the two VMI spectrometers, we use the definitions of the resolution [41],

$$\Delta E/E = 2(\Delta r/r) \times 100\% \quad (1)$$

where Δr is the width of the rings in the image, and r is the radius of the rings. Fig. 4(d) shows a comparison of the KE resolution between the two VMI spectrometers. For the traditional VMI, the "v" shaped dispersion can be clearly found, i.e., the resolution of the medium KE is better and the resolution of the low and high KE is worse [38]. This is because only the ions with the medium KE are focused on the detector plane. For the AL-VMI spectrometer, the ions of the whole KE range are focused on the detector plane. Therefore, from the resolution curve of the AL-VMI in Fig. 4(d), one can find that the resolution keep nearly unchanged with the increase of the KE. A Comparison between the traditional VMI and the AL-VMI shows that the resolution is obviously improved for the low and high KE using the AL-VMI spectrometer. Based on the above simulation, one can see that the KE resolution of the AL-VMI can be improved up by 9% at the energy of 0.5 eV in Fig. 4(d).

3. Experiments

In the AL-VMI, a stepped voltage is needed to apply on the extractor electrode to compensate the spherical aberration of the electrostatic lens. To perform this stepped voltage, we used a fast High voltage Transistor Switch (HTS) made by BEHLKE, and a home-built additional circuit. The circuit used in our experiment is given in Supplementary material [44] published with this paper. To control the turn on-off of the HTS, we used a TTL signal produced by

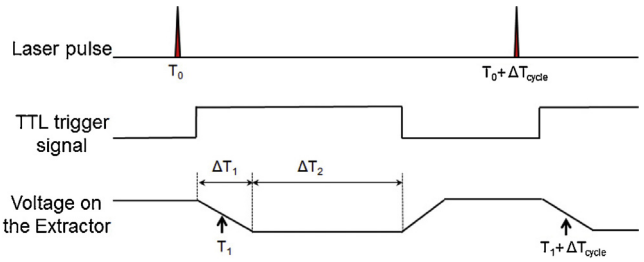

Fig. 5. The timing match of the stepped voltage and its TTL control signal with the laser pulse. $T_0 = 0$, which is the time origin, at which the ionization/dissociation occur. ΔT_{cycle} is the interval of two adjacent laser pulses, which is determined by the laser pulse repetition frequency. We define T_1, which is the midpoint of the step duration, as the time of the step of the voltage. ΔT_1 is the duration of the falling edge of the voltage and ΔT_2 is the duration of V_3. $\Delta T_1 + \Delta T_2$ should be greater than the time of flight of the ions.

a digital pulse generator (DG535, made by Stanford Research Systems). The HTS is turned on at the rising edges of the TTL signal, and turned off at the falling edges. By tuning the starting time of the rising edge, we can tune the starting time of the step of the voltage.

Fig. 5 shows the stepped voltage and the timing match of the TTL control signal with the laser pulse signal. T_0 is the time when the ionization occurs. Hence, we assume that T_0 is the time origin and T_1, the midpoint of the falling edge, is the time of the voltage step. ΔT_1 is the duration of the step process of the voltage and ΔT_2 is the duration of the voltage after the step process. $\Delta T_1 + \Delta T_2$ should be greater than the time of flight of the ions. ΔT_{cycle}, which is the cycle of the voltage pulse, is decided by the laser pulse repetition frequency. In our experiment, the repetition frequency is 1 kHz and $\Delta T_{cycle} = 1$ ms.

To demonstrate the feasibility of the AL-VMI, we have measured the momentum distributions of H^+ produced by the fragmentations of H_2. Briefly, the experimental setups are described as follows. The laser pulses we used were delivered from a Ti: sapphire laser system at a repetition rate of 1 kHz. The pulses are centered at 800 nm and have a pulse width (FWHM) of ~35 fs. The pulses are focused into the interaction region of the VMI spectrometers by a convex lens ($f = 40$ cm). The laser intensity is estimated to be 2×10^{14} W/cm^2. The H_2 molecules first expand through a pulse valve (made by Parker) with an orifice of 0.5 mm. The pulse valve was operated with an opening time of 1 ms at 70 Hz repetition rate. Then, the molecular beam was collimated by a 0.5 mm diameter skimmer. After passing through the skimmer, the molecules spread and go through the hole of the repeller electrode to interact with the laser beam. H^+ ions are produced by the laser interaction with the H2 molecules. The ions are subsequently focused by the electric field onto a dual multichannel plate (MCP, Tectra), followed by a phosphor screen and a CCD camera (Hamamatsu, ORCA-FLASH4.0 LT). The voltage we applied on the MCP is 1.3 kV and on the phosphor screen is 4.7 kV. The channel density of the MCP is about 7×10^5/cm^2 and the pixel density of the CCD camera is about 2.37×10^7/cm^2. The setup of the spectrometer is identical with that in our simulations. The voltage we applied on the repeller electrode is 500 V which is half of the repeller's voltage in the simulation. This is because that the KE release of the H^+ in our experiment is less than 5 eV which is about half of the maximum KE in the simulation. Therefore, to obtain a higher resolution, we applied a small voltage of 500 V on the repeller electrode.

To compare the KE resolution of the traditional VMI with the AL-VMI, we apply a constant voltage and a stepped voltage on the extractor electrode, respectively. For the traditional VMI, the voltage applied on the Extractor is 440 V. For the AL-VMI, the voltage applied on the extractor is a stepped voltage, i.e., the voltage is ini-

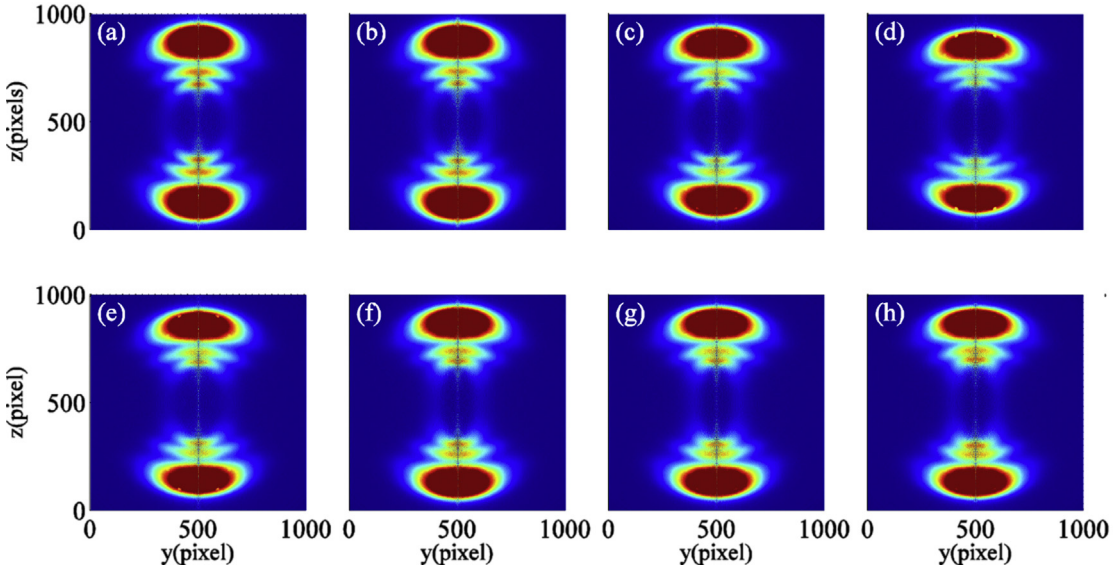

Fig. 6. Experimental results: the images after reconstruction detected by the AL-VMI with T_1 of 24 ns, 44 ns, 64 ns, 84 ns, 94 ns, 104 ns, 114 ns and 124 ns respectively.

tially 500 V and is switched to 400 V at a specific time T_1. In the experiment, we have shortened the duration of the falling edge of the voltage (ΔT_1) by adjusting the resistances and the capacitances of the circuit. The shortest duration of this voltage is 150 ns. Even though the duration is relatively longer compared with that we used in the simulation, the spherical-aberration can still be largely compensated by adjusting the time of the step of the voltage (T_1). In fact the step duration can be as short as 20 ns with a HTS [45]. In our experiment, the large ΔT_1 comes from the fact that the operation voltage of the HTS in our experiment is very small (~500 V).

We investigate the performance of AL-VMI by measuring the fragments of H_2 with the spectrometer. The images after reconstruction are shown in Fig. 6. Fig. 6(a)–(h) show the inverted images by the AL-VMI with T_1 of 24 ns, 44 ns, 64 ns, 84 ns, 94 ns, 104 ns, 114 ns and 124 ns respectively. In all plots, three-ring structures can be clearly seen. The outmost ring is from the Coulomb-explosion channel $H^+ + H^+ + 2e^-$ and the inner two rings are from the dissociative ionization channel $H + H^+ + e^-$ [11]. The central position of the rings is shifted because the field is changed, which has little effect on our discussion. We are more interested in the thickness of the rings, which is directly related to the energy resolution. By comparing the thickness (Δr) of the rings in Fig. 6, one can find that the resolution first gets better and then gets worse as the T_1 is increased. When T_1 is within 60–90 ns, the KE resolution is highly improved. Fig. 7(a) and (b) show a comparison of the images detected by the traditional VMI and AL-VMI (T_1 = 84 ns). One can find that the rings are sharper in the image detected by the AL-VMI than that by the traditional VMI, which indicates that the resolution is obviously improved with the AL-VMI. Then we investigate the influence of T_1 on the resolution. Fig. 7(c) shows the resolution of the second ring with different value of T_1. In Fig. 7(c), the KE resolution first gets better and then gets worse as the increase of T_1. When T_1 is within 60–90 ns, we get the best resolution. In addition, the KE resolution of the second ring of the traditional VMI is also shown in Fig. 7(c). Comparing with the traditional VMI, the KE resolution of the AL-VMI is much better. Thus the KE resolution can be improved obviously with the AL-VMI method. Experimentally, the resolution of the AL-VMI has been improved by 6% as compared with the traditional VMI at T_1 = 64 ns in Fig. 7(c).

From Figs. 6 and 7, one can find that the resolution of the AL-VMI is greatly influenced by the instant of the voltage. The resolution is the best when T_1 is within 60–90 ns. With a simulation in SIMION, we find that the H^+ ions just crossed the extractor electrode at this moment. This is because the stepped voltage is applied on the extractor electrode. Only when the ions cross the extractor electrode, the stepped voltage has a large influence on the trajectories of the ions. Thus the spherical aberration effect can be corrected and the KE resolution can be improved.

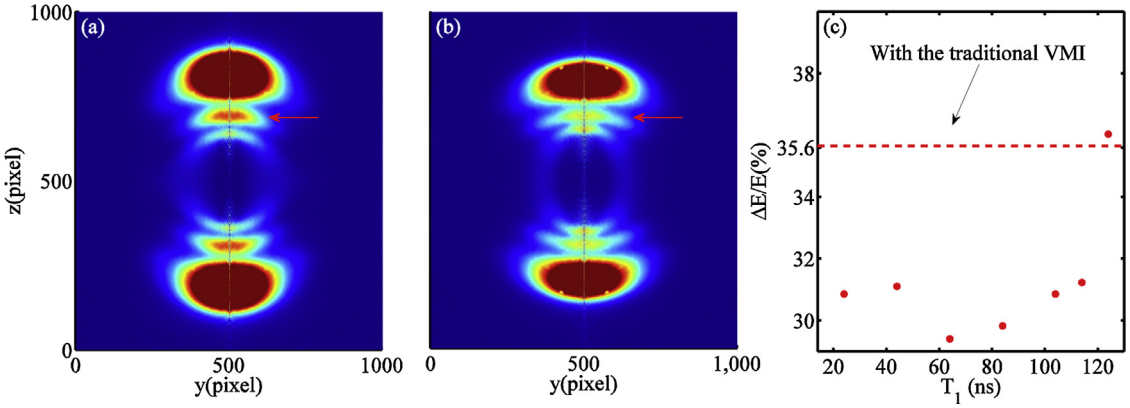

Fig. 7. Experimental results: the images after reconstruction detected by (a) the traditional VMI and detected by (b) the AL-VMI with T_1 = 84 ns. (c) the resolution of the second ring with different T_1.

4. Discussion and conclusion

We find that the improvement of the KE resolution in experiment is not as large as that in the simulation. The large step duration in experiments is mainly responsible for this difference. To get a better KE resolution, the step duration should not be very large. This is because the slope of the voltage during the step process is inverse proportional to the duration of the stepped voltage. In principle, a large slope is necessary for good compensation of the spherical aberration effect. In our experiments, the step duration of 150 ns is relatively large, thus the slope of the stepped voltage is relatively small. To increase the slope in the experiments, we have enlarged the voltage difference of the step process. However, the voltage on the extractor electrode should not be larger than the voltage on the repeller electrode. Therefore, a shorter step duration is still needed to further increase the slope of the stepped voltage. As far as we known, the rise or decay time of the voltage as short as 10 ns can be obtained by a high voltage pulser [46]. With a shorter step duration, the performance of the AL-VMI will be better. In addition, the jitter of the voltage during the step process in the experiments might also affect the performance of the AL-VMI. The voltage jitter comes from the oscillation noise of the circuit which is used to control the on/off of the HTS. Moreover, the actual focus position in experiments is not as perfect as that in the simulation. This may also lead to the different performance of the AL-VMI between the experiment and the simulation. In fact, the optimum timing of the stepped voltage should be adjusted for different masses of ions because their time-of-flight is different. However, the optimum timing of the falling edge of the stepped voltage is determined by the time when the ions fly through the extractor electrode. This conclusion is independent on the mass of the ion.

This method still has a limitation for the photoelectrons. Due to the small mass of the electrons, they would be accelerated to a high velocity in a very short time by the voltage on the repeller electrode. To significantly change the focus of these high-speed electrons, the step of the voltage should be completed in a quite short time ($\sim$1 ns). Otherwise, the electrons would be hardly influenced by the stepped field when the electrons fly through the extractor plate. It is quite difficult to have such a short stepped voltage of 1 ns. As a result, our method has a minor effect on the photoelectrons. Our method is indeed very simple and effective for the ions, compared with the other designs [39–41].

In summary, we have developed a simple method to improve the kinetic energy resolution using the AL-VMI. By applying a stepped voltage on the extractor electrode, the spherical aberration can be suppressed and the KE resolution can be obviously improved. Both the numerical simulations and the experimental results demonstrate that the performance of the AL-VMI is feasible. The "v"-shaped dispersion of the KE resolution in the traditional VMI can be well compensated by this method. In addition, we find that the performance of the AL-VMI is influenced by the time of the stepped voltage. The KE resolution of the AL-VMI is much improved when the falling edge of the stepped voltage is at the instant when the ions travel across the extractor electrode.

Acknowledgment

This work was supported by the National Natural Science Foundation of China under Grants Nos. 61405064, 61475055, 11234004, and 11422435.

Appendix A. Supplementary data

Supplementary data associated with this article can be found, in the online version, at http://dx.doi.org/10.1016/j.ijms.2016.06.006.

References

[1] P. Agostini, F. Fabre, G. Mainfray, G. Petite, N.K. Rahman, Free-free transitions following six-photon ionization of xenon atoms, Phys. Rev. Lett. 42 (1979) 1127.
[2] D. Shafir, H. soifer, B.D. Bruner, M. Dagan, Y. Mairesse, S. Patchkovskii, M.Y. Ivanov, O. Smirnova, N. Dudovich, Resolving the time when an electron exits a tunnelling barrier, Nature 485 (2012) 343.
[3] Y. Li, P.F. Lan, H. Xie, M.R. He, X.S. Zhu, Q.B. Zhang, P.X. Lu, Nonadiabatic tunnel ionization in strong circularly polarized laser fields:counterintuitive angular shifts in the photoelectron momentum distribution, Opt. Express 23 (2015) 28801.
[4] Th. Weber, H. Giessen, M. Weckenbrock, G. Urbasch, A. Staudte, L. Spielberger, O. Jagutzki, V. Mergel, M. Vollmer, R. Dörner, Correlated electron emission in multiphoton double ionization, Nature (London) 405 (2000) 658.
[5] A.H. Tong, Y.M. Zhou, P.X. Lu, Resolving subcycle electron emission in strong-field sequential double ionization, Opt. Express 23 (2015) 15774.
[6] M. Ma, Y.M. Zhou, P.X. Lu, Multiple recollisions in strong-field nonsequential double ionization, Phy. Rev. A 93 (2016) 013425.
[7] J.J. Macklin, J.D. Kmetec, C.L. Gordon III, High-order harmonic generation using intense femtosecond pulses, Phys. Rev. Lett. 70 (1993) 766.
[8] L.X. He, P.F. Lan, Q.B. Zhang, C.Y. Zhai, F. Wang, W.J. Shi, P.X. Lu, Spectrally resolved spatiotemporal features of quantum paths in high-order-harmonic generation, Phys. Rev. A 92 (2015) 043403.
[9] S. Chelkowski, A.D. Bandrauk, P.B. Corkum, Efficient molecular dissociation by a chirped ultrashort infrared laser pulse, Phys. Rev. Lett. 65 (1990) 2355.
[10] Z. Wang, M. Li, Y.M. Zhou, Y. Li, P.F. Lan, P.X. Lu, Counterintuitive energy shifts in joint electron-nuclear-energy spectra of strong-field fragmentation of H_2^+, Phys. Rev. A 93 (2016) 013418.
[11] J.H. Posthumus, The dynamics of small molecules in intense laser fields, Rep. Prog. Phys. 67 (2004) 623.
[12] Y. Li, M.Y. Qin, X.S. Zhu, Q.B. Zhang, P.F. Lan, P.X. Lu, Ultrafast molecular orbital imaging based on attosecond photoelectron diffraction, Opt. Express 23 (2015) 10687–10702.
[13] A.T.J.B. Eppink, D.H. Parker, Velocity map imaging of ions and electrons using electrostatic lenses: application in photoelectron and photofragment ion imaging of molecular oxygen, Rev. Sci. Instrum. 68 (1997) 3477.
[14] S.N. Vogels, J. Onvlee, S. Chefdeville, A. van der Avoird, G.C. Groenenboom, S.Y.T. van der Meerakker, Imaging resonances in low-energy NO-He inelastic collisions, Science 350 (2015) 787–790.
[15] A. Rouzée, F. Kelkensberg, W.K. Siu, G. Gademann, R.R. Lucchese, J.J. Vrakking Marc, Photoelectron kinetic and angular distributions for the ionization of aligned molecules using a HHG source, J. Phys. B: At. Mol. Opt. 45 (2012) 074016.
[16] J. Fedor, J. Kočišek, V. Poterya, O. Votava, A. Pysanenko, M.L. Lipciuc, T.N. Kitsopoulos, M. Fárník, Velocity map imaging of HBr photodissociation in large rare gas clusters, J. Chem. Phys. 134 (2011) 154303.
[17] Y. Huismans, A. Rouzée, A. Gijsbertsen, J.H. Jungmann, A.S. Smolkowska, P.S.W.M. Logman, F. Lépine, C. Cauchy, S. Zamith, T. Marchenko, J.M. Bakker, G. Berden, B. Redlich, A.F.G. van der Meer, H.G. Muller, W. Vermin, K.J. Schafer, M. Spanner, M. Yu Ivanov, O. Smirnova, D. Bauer, S.V. Popruzhenko, M.J.J. Vrakking, Time-resolved holography with photoelectrons, Science 331 (2011) 61–64.
[18] M.R. He, Y. Li, Y.M. Zhou, M. Li, P.X. Lu, Temporal and spatial manipulation of the recolliding wave packet in strong-field photoelectron holography, Phys. Rev. A 93 (2016) 0334067.
[19] Y.M. Zhou, I.T. Oleg, M. Toru, Near-forward rescattering photoelectron holography in strong-field ionization: extraction of the phase of the scattering amplitude, Phys. Rev. Lett. 116 (2016) 173001.
[20] T. Remetter, P. Johnsson, J. Mauritsson, K. Varjú, Y. Ni, F. Lépine, E. Gustafsson, M. Kling, J. Khan, R. López-Martens, K.J. Schafer, M.J.J. Vrakking, A. L'Huillier, Attosecond electron wave packet interferometry, Nat. Phys. 2 (2006) 323.
[21] P. Johnsson, J. Msuritsson, T. Remetter, A. L'Huillier, K.J. Schafer, Attosecond control of ionization by wave-packet interference, Phys. Rev. Lett. 99 (2007) 233001.
[22] L. Holmegaard, J.L. Hansen, L. Kalhøj, S.L. Kragh, H. Stapelfeldt, F. Filsinger, J. K"upper, G. Meijer, D. Dimitrovski, M. Abu-samha, C.P.J. Martiny, L.B. Madsen, Photoelectron angular distributions from strong-field ionization of oriented molecules, Nat. Phys. 6 (2010) 428–432.
[23] C.Y. Zhai, L.X. He, P.F. Lan, X.S. Zhu, Y. Li, F. Wang, W.J. Shi, Q.B. Zhang, P.X. Lu, Coulomb-corrected molecular orbital tomography of nitrogen, Sci. Rep. 6 (2016) 23236.
[24] L.M. Smith, D.R. Keefer, S.I. Sudharsanan, Abel inversion using transform techniques, J. Quant. Spectrosc. Radiat. Transfer 39 (1988) 367–373.
[25] Vladimir Dribinski, Alexei Ossadtchi, Vladimir A. Mandelshtam, Hanna Reisler, Reconstruction of Abel-transformable images: the Gaussian basis-set expansion Abel transform method, Rev. Sci. Instrum. 73 (2002) 2634–2642.
[26] M.J.J. Vrakking, An iterative procedure for the inversion of two-dimensional ion/photoelectron imaging experiments, Rev. Sci. Instrum. 72 (2001) 4084–4089.
[27] R. Wiehle, B. Witzel, H. Helm, E. Cormier, Dynamics of strong-field above-threshold ionization of argon: comparison between experiment and theory, Phys. Rev. A 67 (2003) 063405.
[28] R.A. Morgan, M.A. Baldwin, D. Ascenz, A.J. Orr-Ewing, M.N. Ashfold, W.J. Buma, J.B. Milan, C.R. Scheper, C.A. de Langeb, Resonance enhanced multiphoton

ionisation (REMPI) and REMPI-photoelectron spectroscopy of carbonyl sulphide and carbon disulphide, Int. J. Mass. Spectrom. 159 (1996) 1–11.
[29] M. Li, P. Zhang, S.Q. Luo, Y.M. Zhou, Q.B. Zhang, P.F. Lan, P.X. Lu, Selective enhancement of resonant multiphoton ionization with strong laser fields, Phys. Rev. A 92 (2015) 063404.
[30] P. Agostini, P. Breger, A. L'Huillier, H.G. Muller, G. Petite, A. Antonetti, A. Migus, Giant Stark shifts in multiphoton ionization, Phys. Rev. Lett. 63 (1989) 2208.
[31] A.T. Georges, P. Lambropoulos, ac Stark splitting in doubly resonant three-photon ionization with nonmonochromatic fields, Phys. Rev. A 18 (1978) 587.
[32] P.E. Batson, N. Dellby, O.L. Krivanek, Sub-ångstrom resolution using aberration corrected electron optics, Nature 418 (2002) 617–620.
[33] R. Fickler, W. Schnitzler, N.M. Linke, F. Schmidt-Kalera, K. Singera, Optimised focusing ion optics for an ultracold deterministic single ion source targeting nm resolution, J. Mod. Opt. 56 (2009) 2061–2075.
[34] W. Li, S.D. Chambreau, S.A. Lahankar, A.G. Suits, Megapixel ion imaging with standard video, Rev. Sci. Instrum. 76 (2005) 063106.
[35] M.L. Lipciuc, J.B. Buijs, M.H.M. Janssen, High resolution slice imaging of a molecular speed distribution, Phys. Chem. Chem. Phys. 8 (2006) 219–223.
[36] M.N.R. Ashfold, N.H. Nahler, A.J. Orr-Ewing, O.P.J. Vieuxmaire, R.L. Toomes, T.N. Kitsopoulos, I.A. Garcia, D.A. Chestakov, S. Wu, D.H. Parker, Imaging the dynamics of gas phase reactions, Phys. Chem. Chem. Phys. 8 (2006) 26–53.
[37] M.M. Harb, S. Cohen, E. Papalazarou, F. Lépine, C. Bordas, Transfer-matrix-based method for an analytical description of velocity-map-imaging spectrometers, Rev. Sci. Instrum. 81 (2010) 125111.
[38] P. Zhang, P.F. Lan, Z.P. Feng, Q.B. Zhang, P.X. Lu, Method to compensate the dispersion of kinetic energy resolution in a velocity map imaging spectrometer, Meas. Sci. Technol. 25 (2014) 105202.
[39] S. Skruszewicz, J. Passig, A. Przystawik, N.X. Truong, M. Köther, J. Tiggesbäumker, K.-H. Meiwes-Broer, A new design for imaging of fast energetic electrons, Int. J. Mass Spectrom. 365 (2014) 338–342.
[40] M. Ryazanov, H. Reisler, Improved sliced velocity map imaging apparatus optimized for H photofragments, J. Chem. Phys. 138 (2013) 144201.
[41] N.G. Kling, D. Paul, A. Gura, G. Laurent, S. De, H. Li, Z. Wang, B. Ahn, C.H. Kim, T.K. Kim, I.V. Litvinyuk, C.L. Cocke, I. Ben-Itzhak, D. Kim, M.F. Kling, Thick-lens velocity-map imaging spectrometer with high resolution for high-energy charged particles, J. Instum. 9 (2014) P05005.
[42] H. Lai, T.R. McJunkin, C.J. Miller, J.R. Scott, J.R. Almirall, The predictive power of SIMION/SDS simulation software for modeling ion mobility spectrometry instruments, Int. J. Mass Spectrom. 276 (2008) 1–8.
[43] G. Schönhense, H. Spiecker, Correction of chromatic and spherical aberration in electron microscopy utilizing the time structure of pulsed excitation sources, J. Vac. Sci. Technol. B 20 (2002) 2526–2534.
[44] See supplementary material at [URL will be inserted] for the circuit to realize the stepped voltage.
[45] C.W. Stoermer, S. Gilb, J. Friedrich, D. Schooss, M.M. Kappes, A high resolution dual mass gate for ion separation in laser desorption/ionization time of flight mass spectrometry, Rev. Sci. Instrum. 69 (1998) 1661.
[46] M. Ryazanov, Ph.D. Dissertation, University of Southern California, Los Angeles, 2012.